

Physical, chemical, and ultraviolet radiative characteristics of aerosol in central Alaska

Melanie A. Wetzel,¹ Glenn E. Shaw,² James R. Slusser,³ Randolph D. Borys,¹ and Catherine F. Cahill²

Received 22 November 2002; revised 21 March 2003; accepted 2 April 2003; published 24 July 2003.

[1] A new long-term monitoring site for providing multiwavelength (ultraviolet through near-infrared) and broadband irradiances has been established at the Poker Flat Research Range, Alaska, in order to assess the impacts of ozone, cloud cover, surface albedo, and aerosol conditions on trends in ultraviolet (UV) radiation reaching the surface.

Targeted field measurements were conducted in the first year of site operation to characterize the properties of aerosols commonly found in the study region. Chemical analysis was used to match aerosol composition to aerosol size distributions and spectral aerosol optical depth (AOD). Results are reported on four air mass types: three springtime examples, including an Asian air mass with Gobi Desert dust, aged industrial pollution from the Arctic, and humid marine air, and a comparative case in late summer.

Aerosol imported to central Alaska from extraregional sources produced small to moderate increases in UV optical depth calculated from direct-beam spectral extinction and a limited reduction in transmittance at UV wavelengths. Marine aerosol in a high-humidity environment produced the largest impact on UV extinction. The Angstrom coefficients and single scattering albedos calculated from the spectral AOD and irradiances and the spectral characteristics of size-specific aerosol absorption measurements showed distinct differences between the aerosol source types, suggesting that even in cases of low aerosol concentration, air mass characteristics influence the spectral and angular distributions of UV radiation that are important for modeling photochemical processes and biological exposure.

INDEX TERMS: 0305 Atmospheric Composition and Structure: Aerosols and particles (0345, 4801); 0365 Atmospheric Composition and Structure: Troposphere—composition and chemistry; 3307 Meteorology and Atmospheric Dynamics: Boundary layer processes; 3359 Meteorology and Atmospheric Dynamics: Radiative processes; **KEYWORDS:** aerosol, ultraviolet, Alaska, radiation, optical, Arctic

Citation: Wetzel, M. A., G. E. Shaw, J. R. Slusser, R. D. Borys, and C. F. Cahill, Physical, chemical, and ultraviolet radiative characteristics of aerosol in central Alaska, *J. Geophys. Res.*, 108(D14), 4418, doi:10.1029/2002JD003208, 2003.

1. Introduction

[2] UV radiation dose creates an ecological risk to the sensitive Arctic biota and human inhabitants of high-latitude climate zones [Bjorn, 1996; United Nations Environment Programme (UNEP), 1998; Helbling and Villafane, 2002]. The simultaneous threat of widespread loss of ice and snow cover from ocean, wetland and tundra regions could amplify the potential impact of UV on marine and terrestrial ecosystems. Depletion of stratospheric ozone and changes in dynamical patterns are causing significant variations in radiative exposure in the UV-B wavelength range (280–320 nm) which induces DNA damage, skin cancers, eye lesions, and suppression of immune system function

[UNEP, 1998]. Madronich and de Gruijl [1993] predicted that continuation of present trends could cause basal skin cell carcinoma (cancer) incidence to increase markedly in the coming decades. An additional 20,000,000 cataracts cases per year over 1985 levels could result even if the Montreal protocols are followed [UNEP, 1998].

[3] Stratospheric ozone concentrations are declining in the northern high latitudes from well-known catalytic reactions with anthropogenic chlorine and bromine compounds [Herman *et al.*, 1996; Bojkov *et al.*, 1998; Hansen and Chipperfield, 1999; Solomon, 1999]. While stratospheric ozone fluctuations are now closely monitored [Herman *et al.*, 1996, 1999; Bojkov *et al.*, 1998; Climate Monitoring and Diagnostics Laboratory, 2002], the mesoscale fluctuations in UV radiation at the surface are less well understood. Even though halogen production is being controlled and levels in the stratosphere are expected to diminish [World Meteorological Organization, 1999], increasing greenhouse gases are predicted to cause cooling of the polar stratosphere resulting in greater frequency of Polar Stratospheric Clouds and further polar ozone reduction [Shindell *et al.*, 1998a, 1998b]. Ultraviolet irradiance levels at Barrow,

¹Division of Atmospheric Sciences, Desert Research Institute, Reno, Nevada, USA.

²Geophysical Institute, University of Alaska, Fairbanks, Alaska, USA.

³Natural Resources Ecology Laboratory, Colorado State University, Fort Collins, Colorado, USA.

Alaska, increased during the period 1991–1996 [Gurney, 1998], but the concurrent changes in cloud cover, ozone, and tropospheric aerosols in the increased UV were not determined.

[4] The geographic, seasonal, and interannual variability of ultraviolet irradiance is strongly modulated by solar zenith angle and ozone in the atmospheric vertical column, concentrated in the stratosphere and, to a lesser extent, troposphere. At the same time, ultraviolet irradiance is also affected by surface albedo [Minschwaner, 1999], cloud [Frederick and Steele, 1995], and aerosol extinction [Wenny *et al.*, 1998]. Aerosol impacts can be significant even for small quantities of particulates as aerosol optical depth increases at shorter wavelengths. Exposure is amplified by multiple reflections between surface and atmosphere in locales where the surface has a high UV albedo (such as snow or ice) and/or in the presence of haze or partial cloud cover which allows multiple reflection [Estupinan *et al.*, 1996]. The northern high latitudes commonly experience aerosol haze conditions [Shaw, 1985, 1995; Shaw *et al.*, 1993] enhanced by long distance transport of pollution [Rahn *et al.*, 1977; Shaw, 1988]. Dust from the Gobi and Taklamakan Deserts and pollution from China and other countries in the region, collectively known as Asian dust, are routinely transported northward across the northern Pacific Ocean and Alaska [Rahn *et al.*, 1977]. The ongoing economic development of Northern Hemisphere countries is likely to result in growth of these pollution sources.

[5] The research described in this article examines the role of aerosol in attenuating ultraviolet radiation in central Alaska. The field investigations include episodes of Arctic, Asian and Pacific air mass incursions, in addition to “background” conditions. Measurements of broadband [Taalas *et al.*, 1997] and spectral [Booth *et al.*, 1994] UV irradiance have been previously conducted at high latitudes. The present study presents data and analysis from a new long-term monitoring site at the Poker Flat Research Range (Poker Flat) located 30 km northeast of Fairbanks, Alaska, operated by the University of Alaska’s Geophysical Institute (GI). The Poker Flat site is mostly pristine except for aerosols that arrive by long-range transport (typically in winter and spring) or are generated by forest fires in the region during summer. Four aerosol source types have been investigated: an Asian air mass containing Gobi Desert dust transported across the northern Pacific, aged industrial pollution transported across the Arctic Basin, cloud-processed marine air from the Gulf of Alaska, and summer background conditions.

2. Measurement Systems and Procedures

[6] Instrumentation for study of spectral irradiances and aerosol properties was installed on the roof of the GI Davis Science Center (elevation 550 m MSL) at Poker Flat Research Range (65.12°N, 147.43°W) during August 2000. The instrumentation includes two Yankee Multi-Filter Rotating Shadowband Radiometers (MFRSRs) for continuous measurement of UV and visible irradiances in several narrow wavelength intervals [Bigelow *et al.*, 1998; Harrison *et al.*, 1994] and a Yankee UVB-1 for broadband UV-B (280–330 nm) irradiances (Figure 1).



Figure 1. Multi-Filter Rotating Shadowband Radiometers (MFRSR) and broadband radiometers at the long-term monitoring site on the roof of the Davis Science Center of the Geophysical Institute, University of Alaska, Poker Flat Research Range.

[7] A targeted field program for aerosol sampling was conducted at Poker Flat during March–April 2001. Measurements included size-resolved aerosol chemical composition and concentrations using instrumentation installed at the GI Climate Monitoring Laboratory (CML) (located within 200 m horizontal distance from the Davis Science Center), profiling of aerosol size distributions and atmospheric state parameters with a tether balloon system based within the valley base area of Poker Flat Research Range, and continuous monitoring of meteorological conditions at locations adjacent to the tether balloon sampling location and adjacent to Davis Science Center.

2.1. Parameters Obtained From Irradiance Measurements

[8] The MFRSR rotating shadow band design provides observations of total and diffuse (and resultant direct) irradiance in 13 narrowband filter channels (300, 305, 311, 317, 325, 332, and 368 nm detectors with a full width at half maximum (FWHM) bandwidth of two nm for the UV-MFRSR, and 415, 500, 610, 665, 862 and 940 nm detectors with 10 nm FWHM bandwidth for the Vis-MFRSR). Total, diffuse, and direct spectral irradiances at 3-min intervals were obtained from the MFRSR monitoring site at the Davis Science Center. Calibrated data from the network’s 31 sites is available at <http://uvb.nrel.colostate.edu/>. The UV channel data are also used for retrieval of vertically integrated column ozone [Gao *et al.*, 2001], spectral total optical depth, spectral aerosol optical depth and Angstrom exponent. The spectral measurements allow correlation of UV extinction to the more commonly measured visible extinction, and the availability of both diffuse and direct irradiances permits estimation of the aerosol single scattering albedo (SSA) [Petters *et al.*, 2003] as well as study of UV exposure from direct-beam versus sky-hemisphere diffuse irradiances.

[9] Aerosol optical depth (AOD) was calculated by subtracting Rayleigh and ozone contributions to the total optical depth at each wavelength. Retrievals are performed

using zero-air mass voltage intercepts determined when at least 10 Langley plots [Harrison and Michalsky, 1994] are available for the time period being analyzed. Irradiance calibrations of the UV channels are performed by the NOAA Central UV Calibration Facility in Boulder, Colorado, and have an estimated uncertainty of about $\pm 5\%$ [Shusser *et al.*, 2000].

[10] Angstrom exponents were calculated from the MFRSR data by linear regression to find the slope of \log_{10} (AOD) versus \log_{10} (wavelength) for the combined UV- and Vis-MFRSR measurements at wavelengths from 325 nm to 860 nm obtained from each 3-min observation time where at least four wavelength channel measurements were available and air mass factor was less than 3. Portable sunphotometers (Solar Light MicroTops and University of Alaska design) also provided ozone column amount, aerosol optical depths and water vapor column amount.

2.2. Aerosol Physical and Chemical Parameters

[11] The physical, chemical and optical properties of the aerosols in four air mass types are evaluated in this study. The aerosol size distributions were obtained over the diameter range from 10 nm to 2000 nm diameter using a scanning mobility particle sizer (SMPS) for the particle diameter range 10 nm to 500 nm and an optical particle counter (Met One, model 237) that size-classified the particles into six cumulative size ranges spanning 300 to 2000 nm diameter. Aerosol particle scattering coefficient (b_{sp}) was monitored continuously with a Weiss nephelometer. Aerosol was sampled at room temperature in the CML facility, typically 20 to 30°C above the ambient outside temperatures of -10 to 0°C, thus effectively reducing relative humidity to well below aerosol deliquescence conditions. Vertical profiles of relative humidity were obtained from twice daily rawinsondes launched from Fairbanks (60 km SW of Poker Flat Research Range), tether balloon profiles from a valley sampling location at Poker Flat, and 10-min surface meteorological measurements near CML, to evaluate when elevated relative humidity conditions were influencing the comparisons of AOD and aerosol size distributions.

[12] Aerosol chemical composition was also determined for a time series of impactor samples. A three-stage DRUM aerosol sampling system [Perry *et al.*, 1999] provided size-segregated chemical measurements. The DRUM sampler was operated on a 42-day continuous cycle (3-hour resolution). The impactor samples were analyzed for inorganics (Na through Pb) by Synchrotron X-ray Fluorescence at the Lawrence Berkeley National Laboratory Advanced Light Source [Cahill *et al.*, 1999], β gauge for mass and UV-visible spectroscopy (based on the Laser Integrating Plate Method of Campbell *et al.* [1995]) for aerosol optical absorption. These techniques are nondestructive to the aerosol samples.

[13] Aerosol chemical composition yields information about probable sources. For example, crustal material such as desert dust is enriched in Al, Si, Ca, Ti and Fe, metal smelting enriches Ni, Cu, and Zn, sea salt enriches Na and Cl, while forest fires are often affiliated with enhancements in K. The chemical measurements were size resolved into “fine” (0.1 to 0.34 μm diameter), “medium” (0.34–1.15 μm diameter), and “large” (1.15 to 2.5 μm diameter) fractions sizes.

[14] Time-extended aerosol measurements were primarily carried out at the surface, but several vertical profiles using an instrumented tether balloon were collected from a valley location within 1 km of the CML and Davis Science Center sites. These provided information on the vertical variability of aerosol concentrations. The profiling system included the Met One size-specific particle counter, a cloud videometer (for deriving microscopic video imagery of ice crystals and cloud droplets if fog occurred) and a radiosonde to measure temperature, relative humidity, atmospheric pressure, wind speed, and wind direction.

3. Results

3.1. Interannual and Seasonal Measurements

[15] Figure 2 presents a 2-year time series of solar noon broadband UV-B (erythemal) irradiance measured at Poker Flat, demonstrating the range in typical midday UV irradiance magnitudes between summer and winter. Large day-to-day fluctuations seen in Figure 2 are associated with periods of cloud cover. The annual range in daylight-integrated UV exposure is controlled at this locale by the high latitude. The sensitivity of UV exposure to ozone column amount is also large due to the seasonal cycle of ozone, which diminishes during the spring and early summer months in this region. A shift in the amplitude or time of minimum ozone, superimposed on a change in regional climate because of early snowmelt or altered cloud cover, could dramatically influence UV exposure for emerging plant life and humans active outdoors during the late spring.

[16] The long path length of the solar beam enhances the effect of aerosol on UV extinction. Through this process, the frequent incursions of haze and dust during spring, and forest fire smoke in summer, help to offset UV exposure during the period when snow albedo is still high in many areas and day length is increasing. However, changes in atmospheric circulation patterns, precipitation or other aerosol source forcing could remove the screening effect of aerosol and increase the risks from persistent exposure to UV.

[17] Aerosol concentrations and size distributions at Poker Flat during the Spring 2001 campaign were relatively constant over periods of hours and even days and usually were low, as was to be expected for a remote site. The time series of aerosol concentrations in six particle diameter size bins is illustrated in Figure 3. The temporal pattern in the nephelometer measurements follows that of the Met One aerosol concentrations (Figure 4), and the scattering coefficient is low (generally $<14 \text{ M m}^{-1}$). The values of particle scattering coefficient correlate well ($R^2 = 0.76$) with the aerosol concentrations.

[18] Profiles of aerosol concentrations, wind, relative humidity and temperature indicated a well-mixed boundary layer for most days studied. With tether balloon data extending more than 1 km from the valley launch site (220 m MSL) and past the CML aerosol sampling site (550 m MSL), the aerosol concentration varied $<10\%$ along the vertical profile in 8 of 10 balloon flights. The two remaining cases during the unsettled weather period of early April showed variations in concentration of 20 and 41%. Aerosol size distributions measured at CML prior to and following the profiles, using the same Met One instrument,

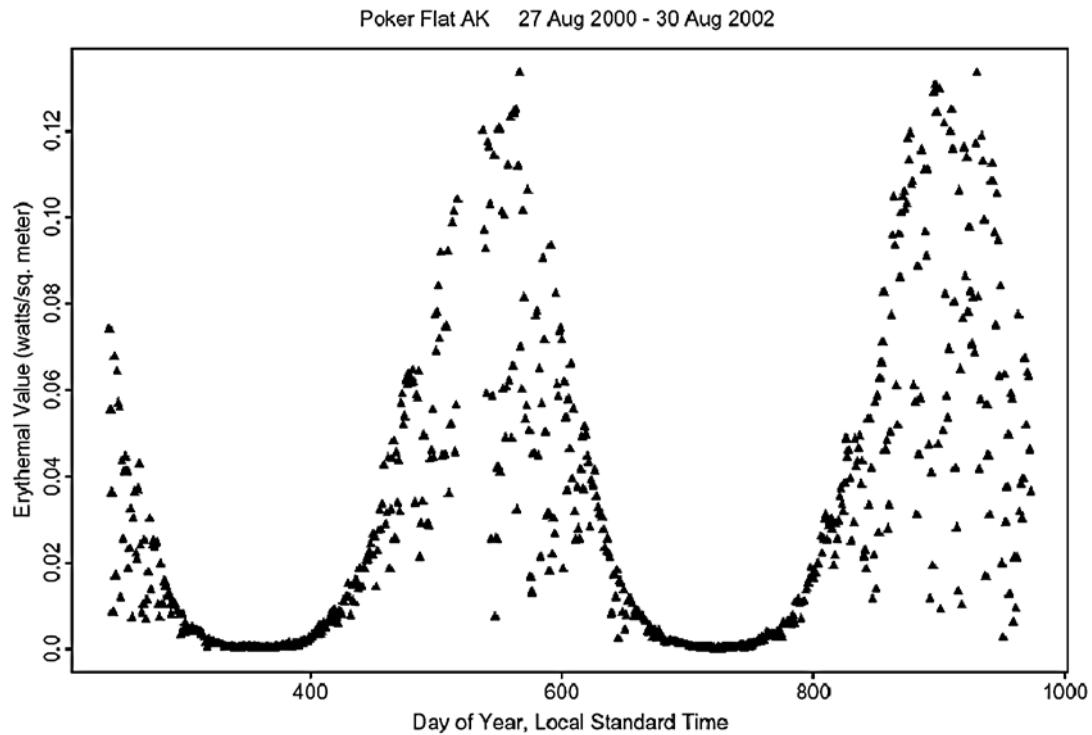


Figure 2. Two-year time series of erythemal irradiance at solar noon from monitoring site at Poker Flat Research Range.

matched those measured from the tether balloon during the profiles, supporting the conclusion that aerosol data measured at the CML were representative of aerosol characteristics in the lower troposphere.

[19] Size-segregated chemical analysis of collected aerosol samples provides information on the sources of aerosol

reaching the study location. Figure 5 presents the time series of the concentrations of four crustal elements found in the medium-sized aerosol (diameter $0.34\text{--}1.15\ \mu\text{m}$) during the March–April 2001 sampling period. Transitions in air mass composition are indicated on 2 April and 16 April, associated with concentration peaks that are evidence

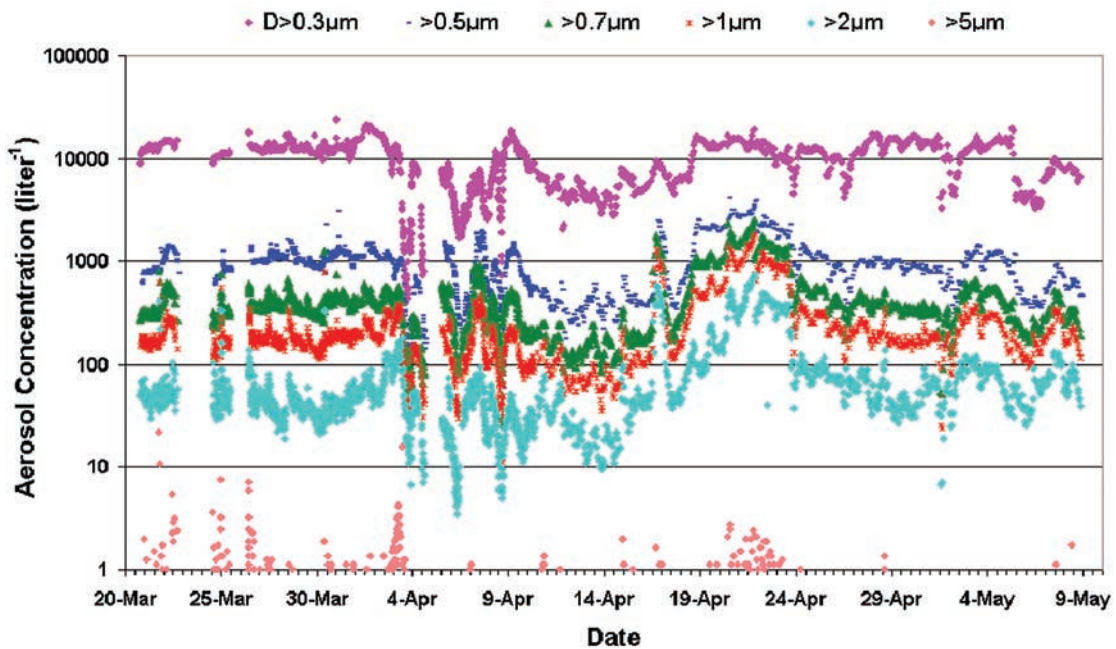


Figure 3. Aerosol number concentrations measured in six cumulative diameter (D) ranges made at the Climate Monitoring Laboratory, Poker Flat, Alaska, during spring 2001.

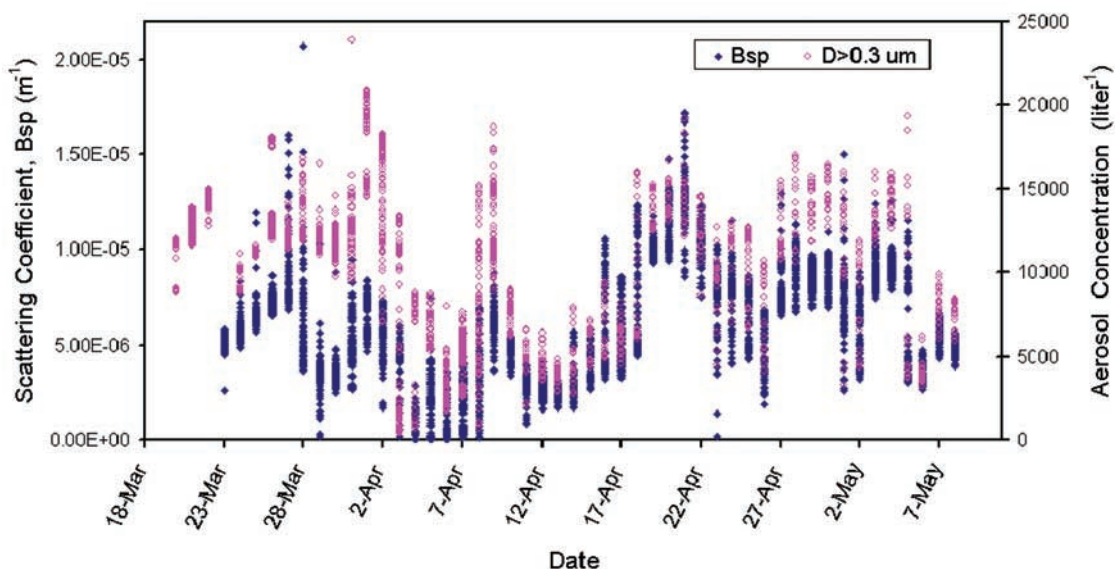


Figure 4. Aerosol number concentrations of aerosols $>0.3 \mu\text{m}$ diameter and aerosol light scattering coefficients made at the Climate Monitoring Laboratory at Poker Flat, Alaska, during spring 2001.

of frontal passages, and shifts in overall concentrations within different airflow regimes. The period 22 March to 2 April (particularly 22–29 March) was a regime of northerly flow with aerosol transport from across the Arctic Basin (Figure 6), the period 2–15 April provided predominantly southerly flow of marine air and was accompanied by precipitation, and the period 15–22 April brought south-

westerly flow with transport from Asia (Figure 7). Measurements of aerosol and radiative conditions within these regimes are discussed in the following section.

3.2. Case-Specific Radiative Parameters

[20] Specific days within the period of springtime field measurements were selected for analysis of the radiative

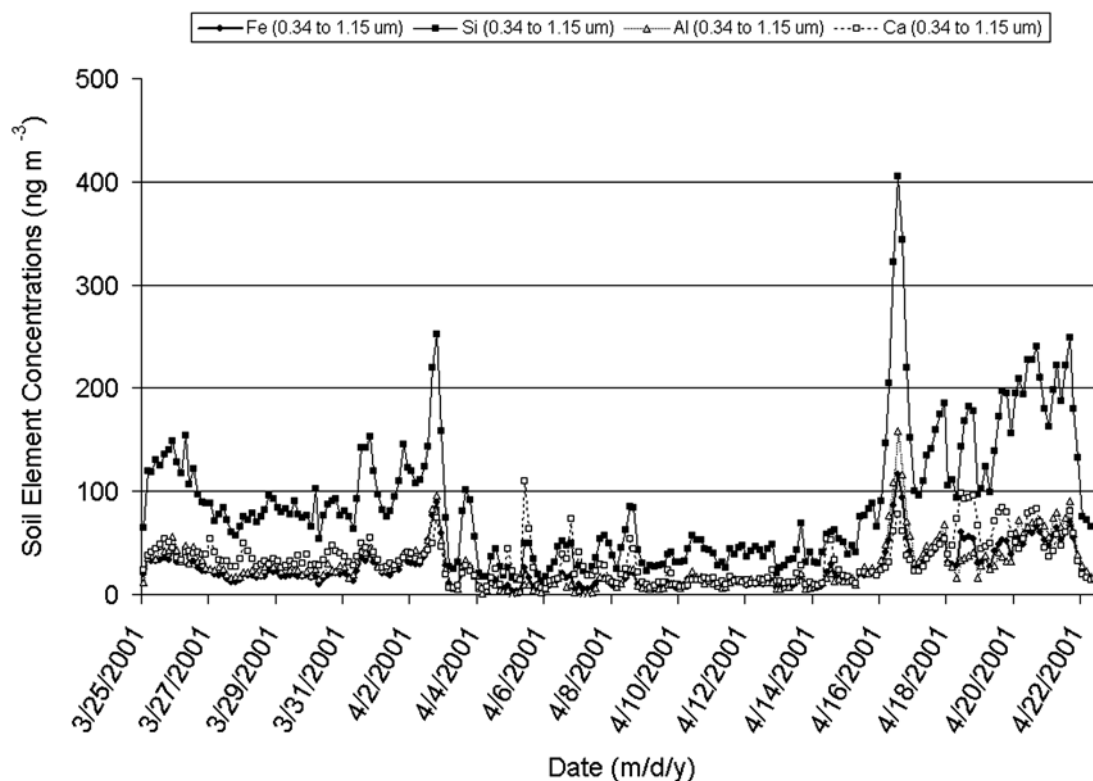


Figure 5. Medium-size fraction crustal elements (iron, silicon, aluminum, and calcium) at Poker Flat from 25 March to 22 April 2001. All times are in Alaska Standard Time (AST).

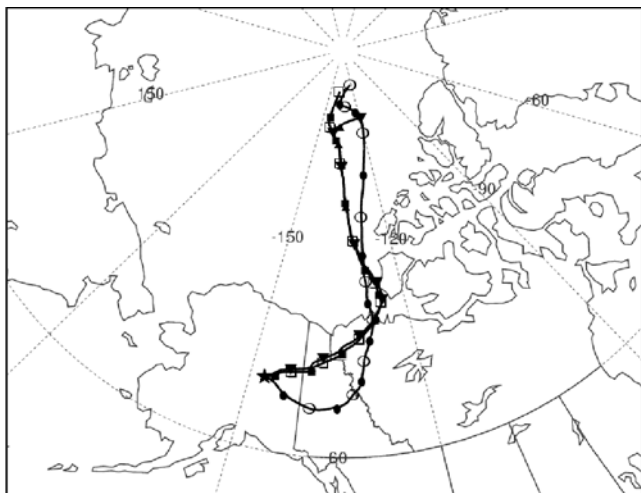


Figure 6. Backward trajectories for air parcels from multiple heights, arriving to Poker Flat, Alaska, at 0000 UTC on 24 March 2001 indicating a deep Arctic air intrusion into central Alaska.

impacts for various air mass types, and these conditions were also compared to a late summer case. The dates were chosen to avoid cloudy periods and to match as well as possible the various types of measurements available (aerosol chemistry, nephelometer, SMPS, Met One, and MFRSR data sets).

[21] Table 1 presents the midday ranges of AOD values at 368 nm, and Angstrom exponents calculated for the AOD measurements between 325 and 860 nm, during 4 days that represent the air mass types. Spectral AOD values and Angstrom exponents are influenced by aerosol number and mass concentrations, aerosol chemical composition, ambient humidity, and the vertical profiles of these parameters. The summer conditions are characterized by low UV AOD, except during forest fire events. A range of low (0.05) to moderate (0.15) AOD conditions were noted

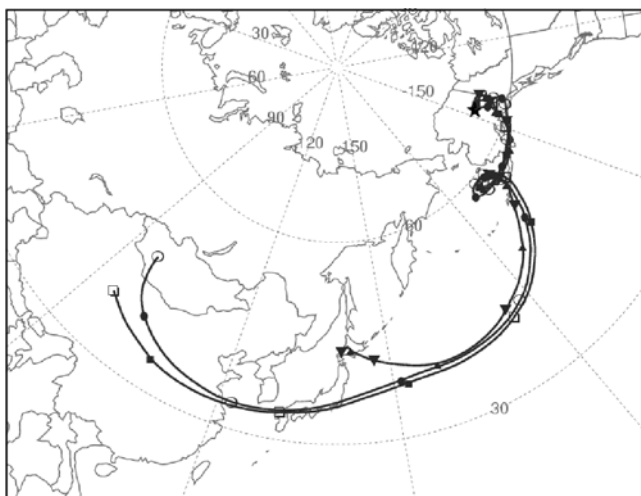


Figure 7. Backward trajectories for air arriving to Poker Flat, Alaska, at 0000 UTC on 16 April 2001 showing transport from Asia during the Asian dust episode to Poker Flat, Alaska.

Table 1. Range of AOD at 368 nm and Angstrom Exponent (325–860 nm) During Midday for Selected Case Study Dates

Mass Type	Date	AOD ₃₆₈ Range	Angstrom Exponent Range
Summer	16 September 2001	0.05–0.06	0.68–0.94
Spring Arctic	22 March 2001	0.05–0.06	0.76–0.99
Spring Asian	19 April 2001	0.11–0.14	0.06–0.15
Spring marine	9 April 2001	0.15–0.25	0.72–0.97

during the spring Arctic air mass period. Arctic haze in the Barrow, Alaska, region typically causes high AOD conditions, but a low-AOD day was selected for analysis during this airflow regime to examine a case which has the chemical and trajectory signature of an Arctic haze episode but low total aerosol loading. This situation can arise from a loss of the majority of Arctic haze constituents during the long-distance transport into central Alaska. AOD₃₆₈ values during the Asian air mass event were double those for the late summer background period and the Arctic source period. During the period of marine air mass influence, AOD₃₆₈ varied considerably and reached some of the highest values observed during the month-long field study. Rawinsonde profiles and surface measurements showed that this period was humid (relative humidity 70–90%) through a deep layer (surface to 3 km).

[22] Angstrom exponent values representing the spectral dependence of extinction were similar (in the range ~0.7–1.0) for the cases of Marine, Arctic and Summer air mass types but were notably smaller for the Asian air mass (<0.2). Smaller values of the Angstrom exponent are likely due to larger particles present in the Asian air mass. Previous studies in Alaska [Quinn *et al.*, 2002] have associated a seasonal increase in the Angstrom exponent from winter to summer with a shift toward smaller particle sizes because of more prevalent biogenic sources and gas-to-particle production.

[23] The Angstrom exponent can be used in calculating model irradiances for spectrally specific processes such as photochemistry (in the free air or at the surface) and biological response functions (such as microbial activity, human skin exposure, etc). Spectral AOD and Angstrom exponents are also useful in estimating the wavelength dependence of transmittance. Table 2 lists transmittance relative to clear-sky conditions with no aerosol as calculated from the DISORT radiative transfer code [Stamnes *et al.*, 1988; Slusser *et al.*, 2002], and applying the AOD and Angstrom exponent derived from midday conditions for the

Table 2. Model Computations of the Solar Noon Spectral Transmittance (T), Relative to No Aerosol Loading, for Measured Aerosol Optical Depths (AOD) at 368 nm and Measured Angstrom Exponent During Four Case Studies^a

Air Mass Type	Date	AOD ₃₆₈	Angstrom Exponent	T ₃₆₈	T ₃₀₅
Summer	16 September 2001	0.06	0.90	0.972	0.972
Spring Arctic	22 March 2001	0.06	0.85	0.973	0.973
Spring Asian	19 April 2001	0.13	0.12	0.951	0.949
Spring marine	9 April 2001	0.25	0.72	0.899	0.887

^aFor all computations the asymmetry parameter was 0.70, single scattering albedo was 0.90, surface albedo was 0.05, and ozone column amount was 300 DU.

Table 3. Single Scattering Albedo (SSA) Estimated From the Ratio of Direct to Diffuse Irradiances at 368 nm^a

Air Mass Type	Date	AOD ₃₆₈	SZA, deg	Surface Albedo	SSA ₃₆₈
Summer	16 September 2001	0.06	62.7	0.05	0.88
Spring Arctic	22 March 2001	0.05	64.1	0.90	ND ^b
Spring Asian	17 April 2001	0.13	54.6	0.48	0.76
Spring Asian	18 April 2001	0.20	54.3	0.48	0.71
Spring Asian	19 April 2001	0.13	53.9	0.48	0.63
Spring Asian	20 April 2001	0.09	53.6	0.48	ND ^b
Spring marine	9 April 2001	0.25	57.2	0.90	0.95

^aAlso indicated are the aerosol optical depth values (AOD) at 368 nm, the solar zenith angle (SZA) at the measurement time (solar noon), and the estimated UV surface albedo.

data set shown in Table 1. The model calculations indicate that UV transmittance decreased 3–10% at 368 nm and 3–11% at 305 nm because of the presence of aerosol during these four events. The calculations in this example were performed with a low value for ozone column amount (300 DU). Less sensitivity to the ambient AOD conditions would be found for the shorter UV wavelengths in situations with the higher ozone column amounts that typically occur in springtime. The most significant reductions in transmittance were associated with the marine air mass.

[24] The single scattering albedo for an ambient aerosol population can also be estimated from the available spectral irradiance measurements. Single scattering albedo is influenced by several factors including aerosol composition, size, shape and the ambient relative humidity [Reuder and Schwander, 1999; Petters *et al.*, 2003]. Dust particle populations have been assigned values as low as 0.55 but increasing to 0.90 as particle size decreases [Torres *et al.*, 1998; Sokolik and Toon, 1999]. Carbonaceous aerosol populations are associated with moderate values (0.85–0.95), while marine and other sulfate-containing aerosol have high values (0.90–1.00) [Torres *et al.*, 1998; Li *et al.*, 2001]. Hofzumahaus *et al.* [2002] estimated values of UV-band SSA as 0.95 and 0.87 on 2 summer days from an island in the Aegean Sea (40°N), by finding best fit values of SSA between measured and modeled AOD. Petters *et al.* [2003] used a radiative transfer model to match direct-to-diffuse irradiance ratios from a UV-MFRSR (located at 36°N in the eastern United States) to estimate SSA in the UV. Their values of SSA ranged from 0.81 to 0.99 at 368 nm and from 0.71 to 0.96 at 305 nm. An analysis of back trajectories revealed no correlation between the SSA and the origin of the air mass 48 hours prior to measurement, which was interpreted as evidence of multiple aerosol source distributions along the trajectories.

[25] The Petters *et al.* [2003] technique is used to produce SSA estimates shown in Table 3. In two of the cases, ND is indicated where the retrieval was not possible because of high surface albedo or low AOD conditions that overwhelm the direct-to-diffuse ratio sensitivity to SSA. AOD values were obtained from the MFRSR measurements and surface albedo was estimated from satellite data. Weihs *et al.* [2001] and Kylling *et al.* [2000] discuss methods for computing an effective albedo for inhomogeneous surfaces, which could be usefully applied when conditions of higher AOD warrant

this refinement. The cases for which SSA was estimated indicate high values for the marine air mass and relatively low values for the Asian air mass, corresponding to the expected differences due to aerosol sources (marine sulfate versus moderate-size dust particles) as discussed above.

3.3. Intercomparison of Air Mass Types

3.3.1. Summer Background Air Mass

[26] Late summer to early autumn is typically the time of lowest aerosol concentrations and impacts on visual extinction at Poker Flat [Quinn *et al.*, 2002]. A representative late summer case was chosen during September 2001 for comparison to the springtime cases. AOD values at 368 nm were 0.06 or less for the entire day of 16 September 2001 and calculated transmittance was 97% of that for no-aerosol conditions (Table 2). The Angstrom exponent calculated from the visible and near-UV AOD values was 0.9, higher than in the Arctic air mass, suggesting a predominance of small particles. The estimated aerosol SSA this day (Table 3) was 0.88, which despite the small AOD was retrievable using the direct-to-diffuse irradiance ratio technique due to low surface albedo conditions in late summer.

3.3.2. Arctic Air Mass

[27] A strong incursion of arctic air to interior Alaska occurred during late March 2001. A calculated air parcel trajectory (Figure 6) shows that this originated from the central Arctic Basin. During this period of arctic air influence, the surface temperatures at Poker Flat were several degrees below seasonal mean. Although the AOD at Poker Flat was low, the Fairbanks area experienced degraded visibility due to the combined effects of urban aerosol sources and valley inversion conditions.

[28] The chemical composition showed elevated concentrations of metals (Figure 5) and sulfur (Figure 8) indicative of Arctic haze. Large peaks in fine particle metals and other anthropogenic compounds occurred during the last week of March (Figures 9 and 10). The aerosol number concentration remained relatively constant during this period. The SMPS size distribution was monomodal (Figure 11) with no detectable nucleation mode. Peak concentrations of aerosol were lower than for the Asian air mass, both as observed by the SMPS (Figure 12) and the Met One (Figure 3). AOD values and impacts on UV transmittance were less than those for the Asian air mass (Table 2). No estimation of aerosol SSA was made in this case because of small AOD and high surface albedo.

[29] The spectral character of the aerosol relative absorption (Figures 13a–13c) is indicated to vary inversely with particle size. The larger particles absorb more incident radiation at 350 nm than 750 nm, while the smaller particles absorb at 750 nm more effectively. The total relative absorption measured by UV-visible spectroscopy of the aerosol impactor samples (Figure 13d) follows the aerosol chemical concentration patterns (i.e., when elemental concentrations are high, total relative absorption is high). During the Arctic air mass period, the total relative absorption was generally dominated by absorption from the 0.34- to 1.15- μm aerosol size fraction. This is consistent with the aerosol chemical concentration results during this event that show the 0.34- to 1.15- μm - aerosol size fraction sulfur and other anthropogenic components composing most of the observed aerosol mass. Although large aerosol account for a small component of

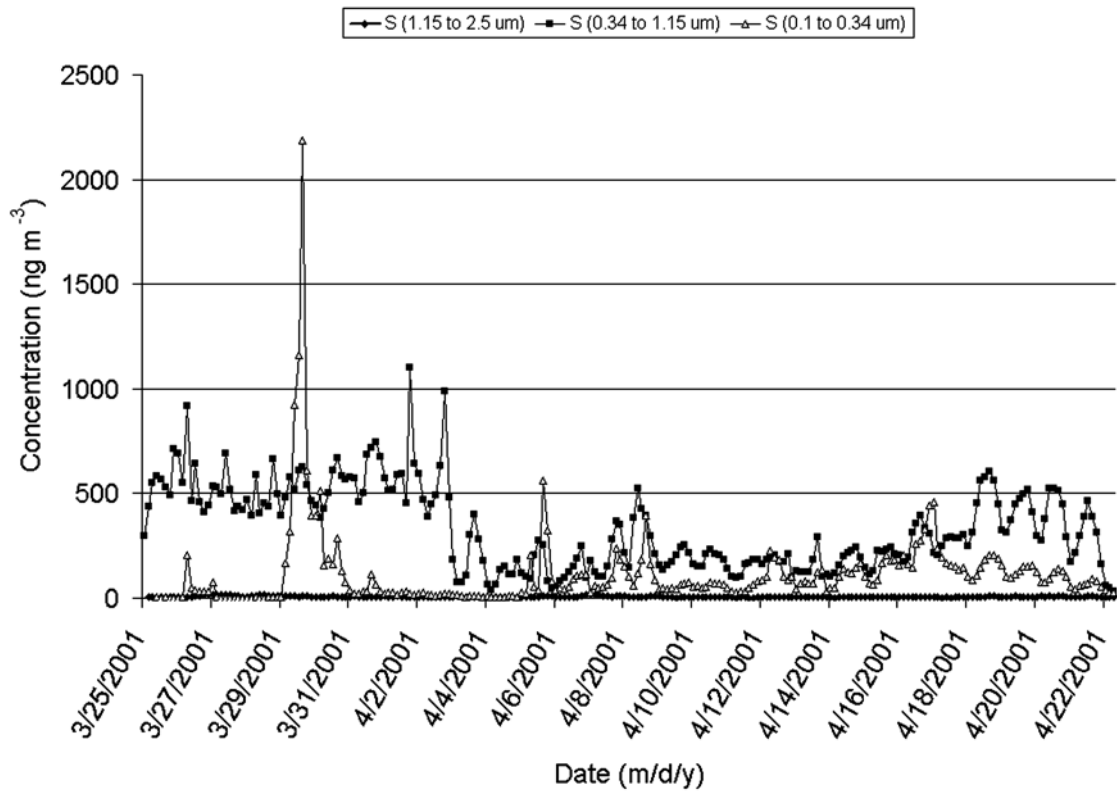


Figure 8. Fine-, medium-, and large-size fraction sulfur at Poker Flat from 25 March to 22 April 2001.

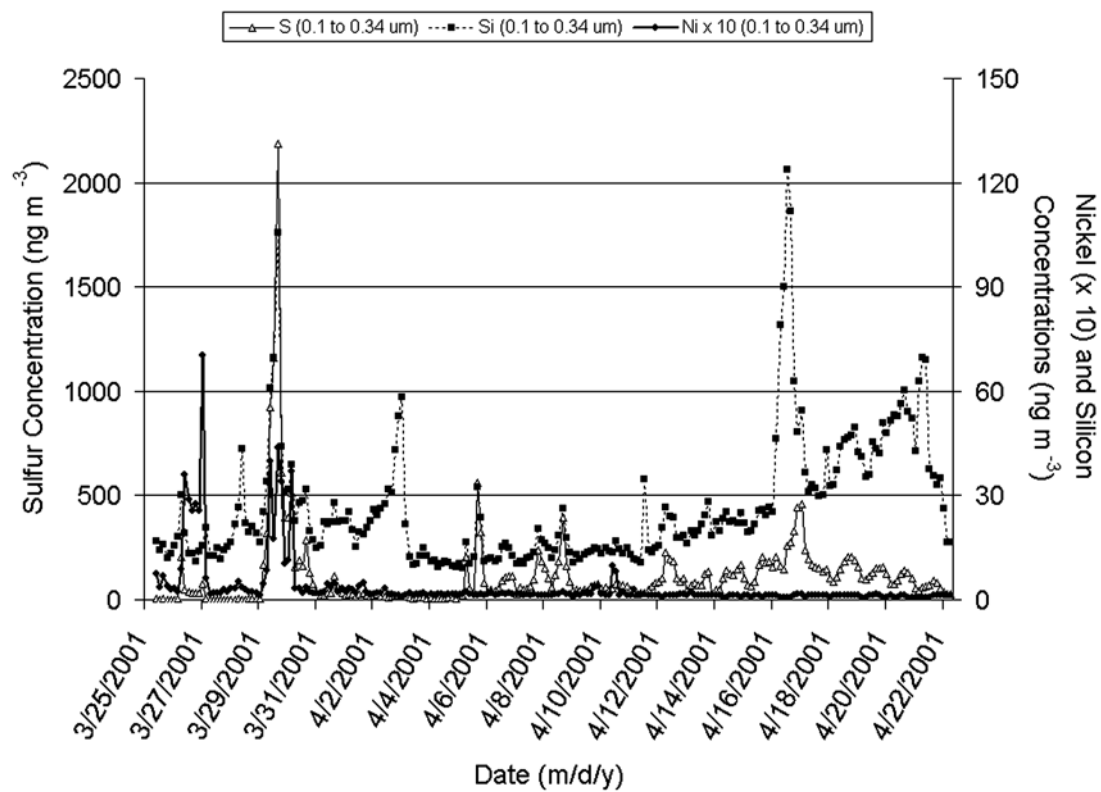


Figure 9. Fine-size fraction sulfur, silicon, and nickel (the nickel concentration is multiplied by 10 on the y axis) at Poker Flat from 25 March to 22 April 2001.

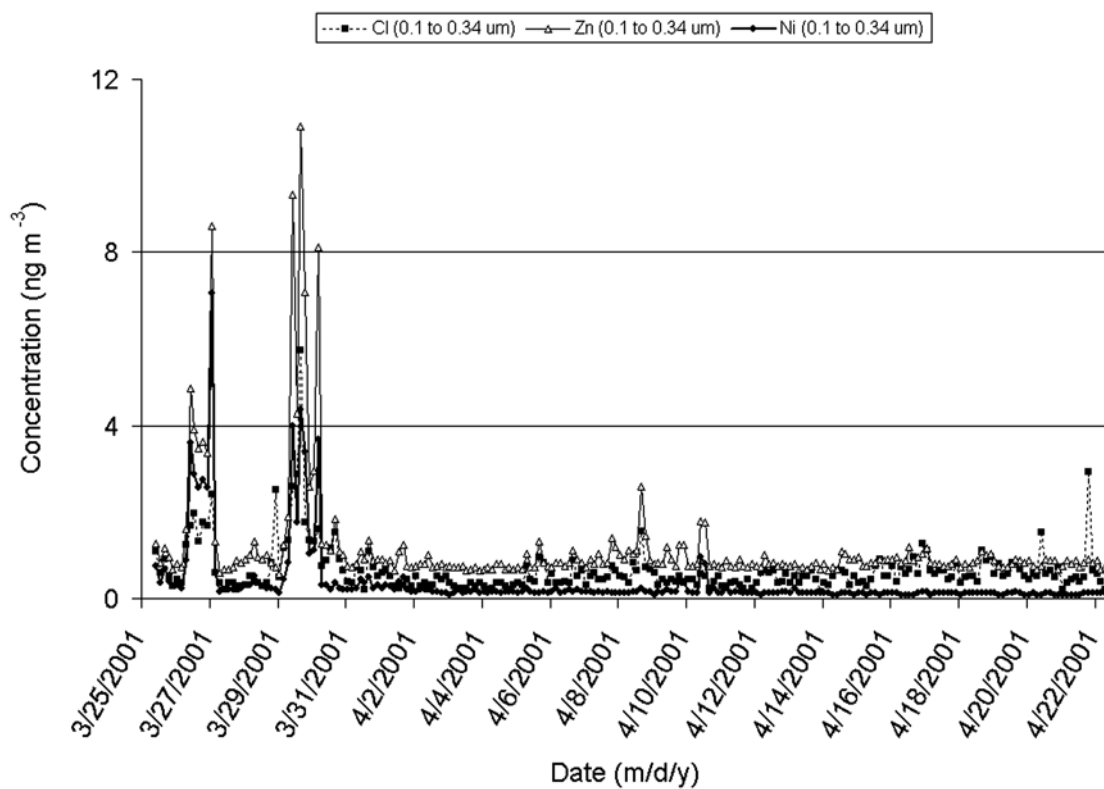


Figure 10. Fine-size fraction chlorine, zinc, and nickel at Poker Flat from 25 March to 22 April 2001.

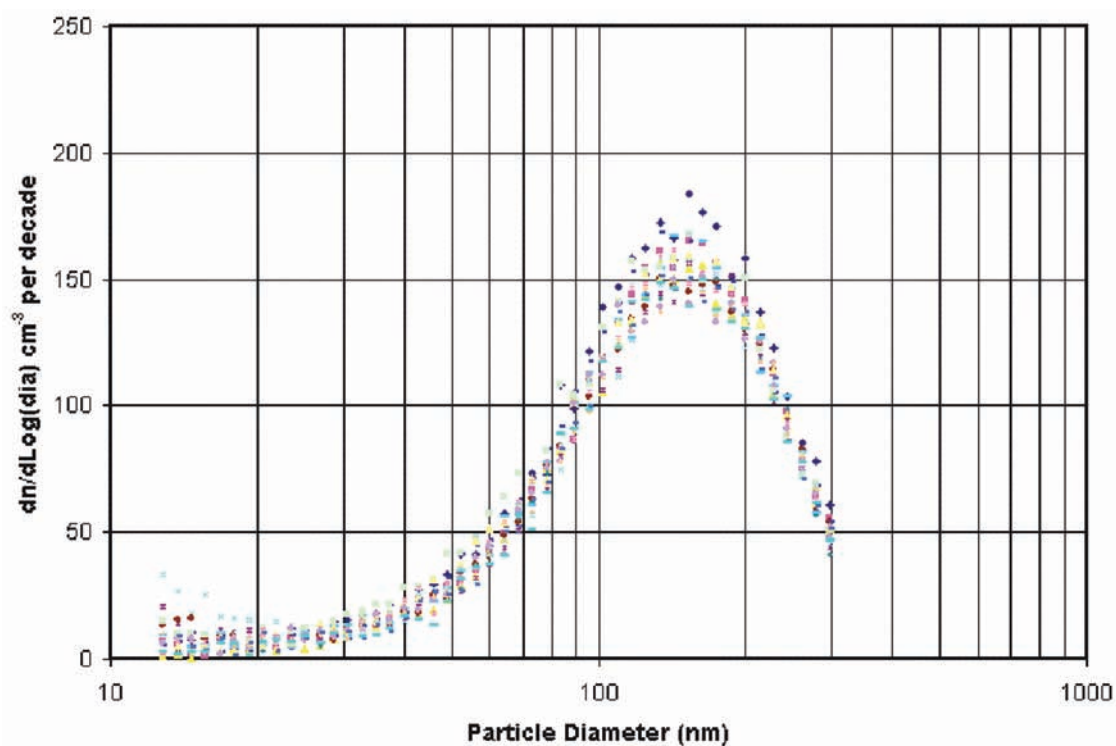


Figure 11. A series of aerosol size distributions on 23 March 2001 representing Arctic haze during a cold air mass incursion from the north to Poker Flat, Alaska.

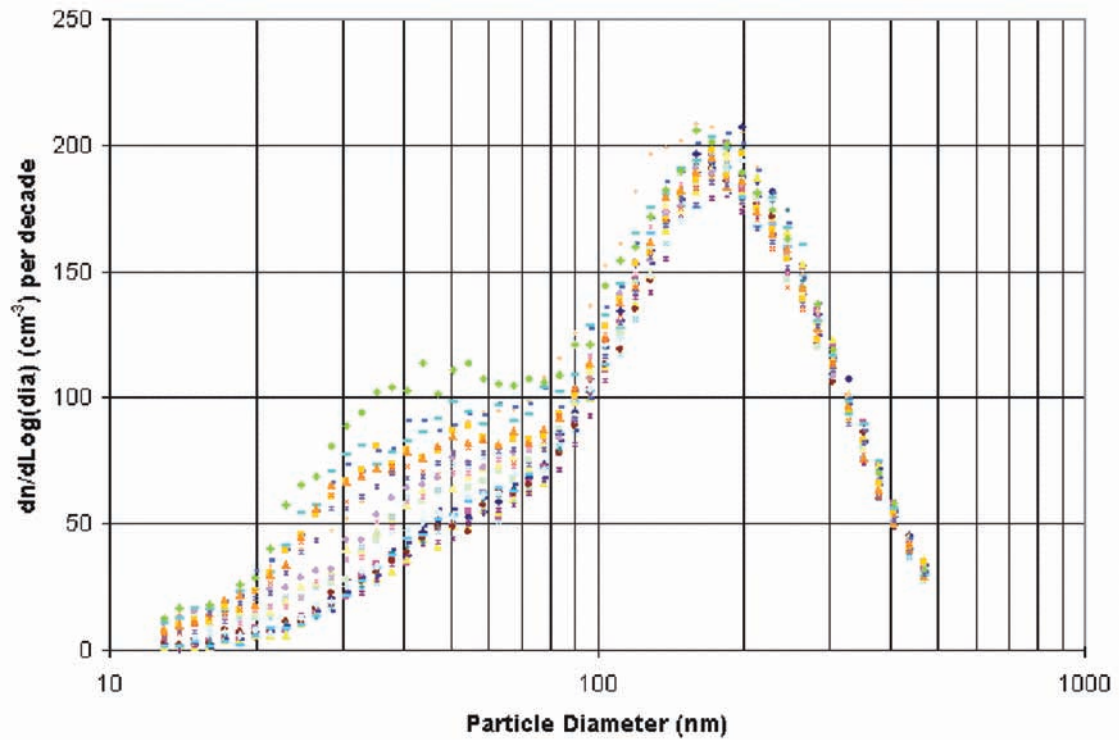


Figure 12. A series of aerosol size distributions on 19 April 2001 representing the Asian dust intrusion period.

the total absorption, the particles in this size range are effective UV absorbers. Future analysis of these absorption measurements with respect to the mass loading and number concentrations in the three size ranges will provide additional information regarding the wavelength-

and size-specific extinction properties of the aerosol types.

3.3.3. Asian Air Mass

[30] A buildup of aerosol concentration (Figure 4) during the period 15–22 April is associated with incursion of an

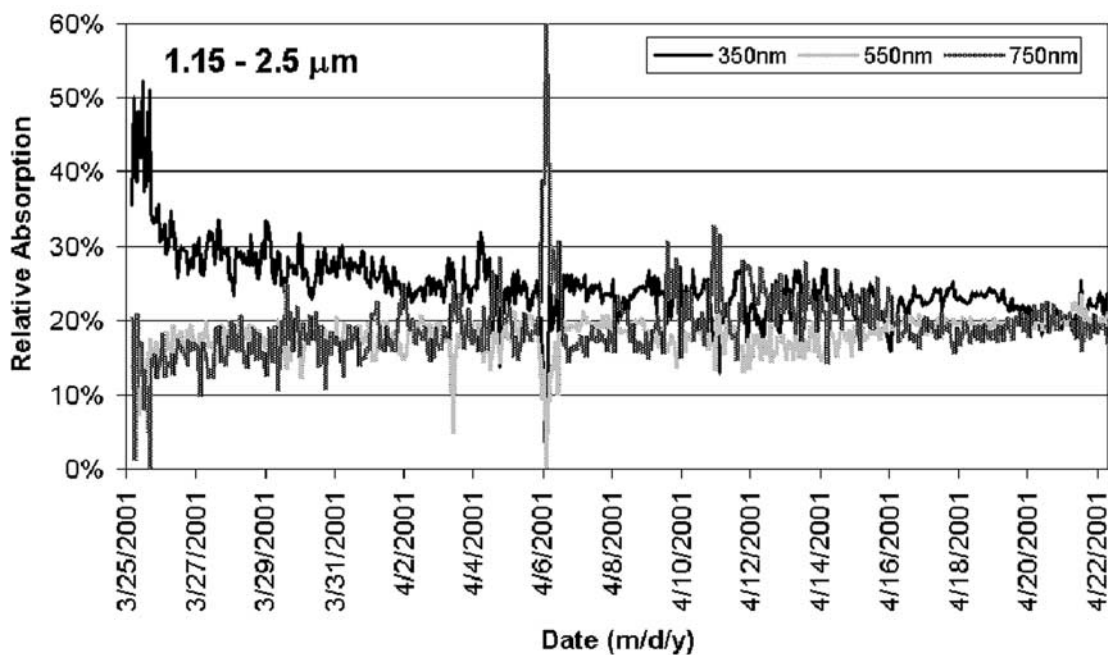


Figure 13a. Aerosol optical absorption at 350 nm, 550 nm and 750 nm determined using the Laser Integrating Plate Method from impactor samples of aerosol collected at Poker Flat Research Range, Alaska, for 1.15–2.4 μm aerodynamic diameter.

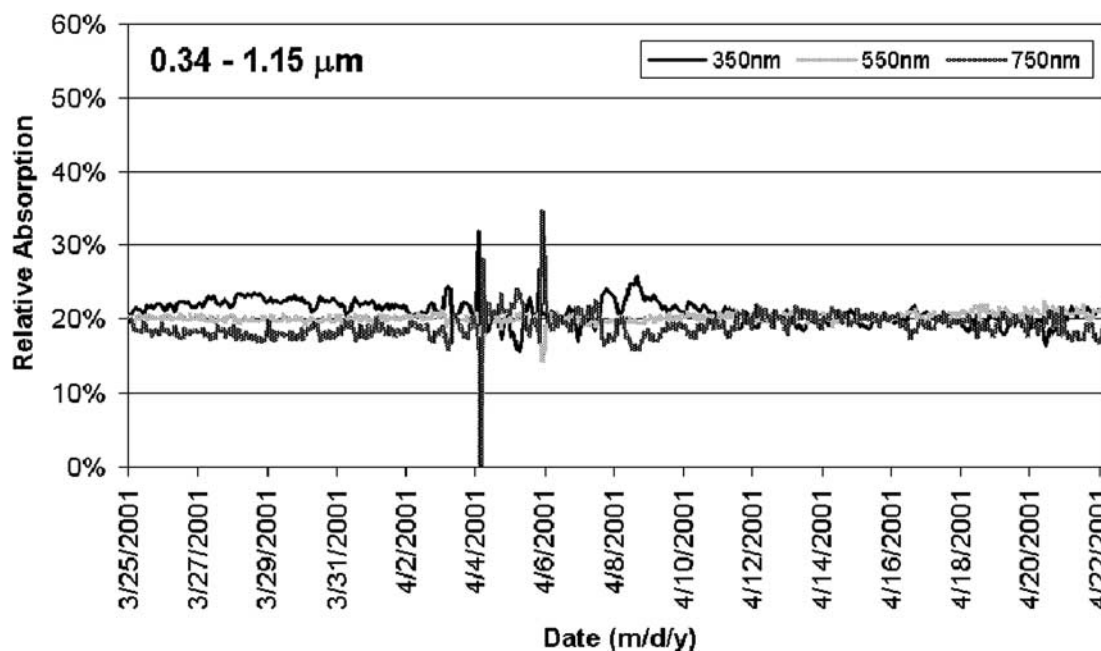


Figure 13b. Same as Figure 13a but for 0.34–1.15 μm aerodynamic diameter.

Asian air mass containing dust from the Gobi Desert. A backward trajectory shows the Asian source region (Figure 7). During this incursion the size distribution measured by the SMPS (Figure 12) was dominated by a mode centered near 160 nm, with some occasional number enhancements near 50 nm diameter. There were large increases in the concentrations of crustal aerosol (Figure 14) with smaller increases in anthropogenic components such as S (Figure 9). Table 3 shows the aerosol SSA estimated at 368 nm for 17–19 April assuming a surface albedo of 0.48. The SSA results

ranged from 0.63 to 0.76 and are consistent with SSA values for small-size dust aerosol as parameterized by *Torres et al.* [1998]. The total relative aerosol absorption during this period shows the greatest attenuation observed during the study (Figure 13d). The total relative aerosol absorption follows the temporal pattern of the large soil particles in the 1.15- to 2.5- μm -size fraction and the sulfur in the 0.1- to 0.34- μm -size fraction. The middle-size fraction shows peaks that correlate with both the anthropogenic and soil components. The spectral absorption measurements suggest some-

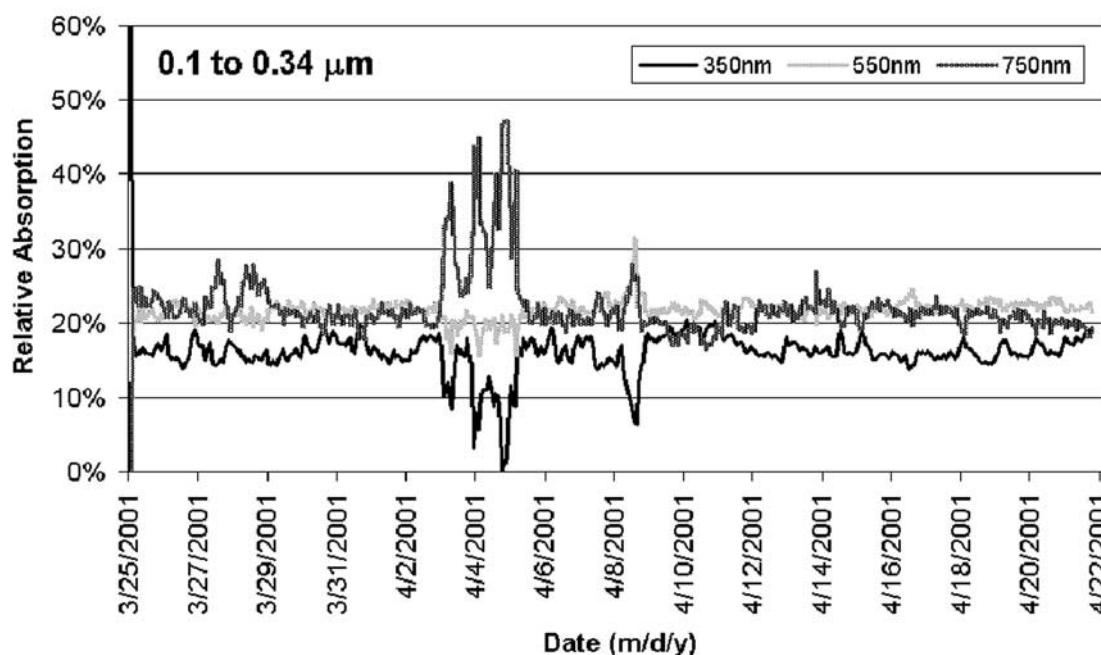


Figure 13c. Same as Figure 13a but for 0.1–0.34 μm aerodynamic diameter.

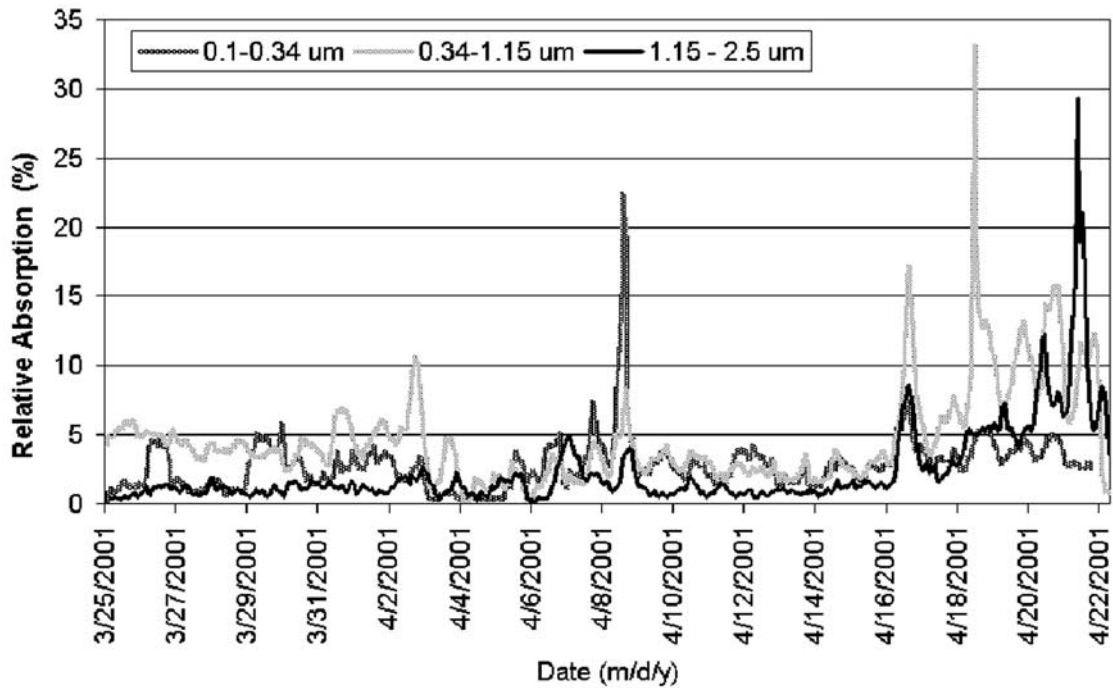


Figure 13d. Total relative absorption, a measure of the total light attenuation due to absorption. Periods with low total absorption generally have more variability in their wavelength-specific percentage relative absorption values in Figures 13a–13c.

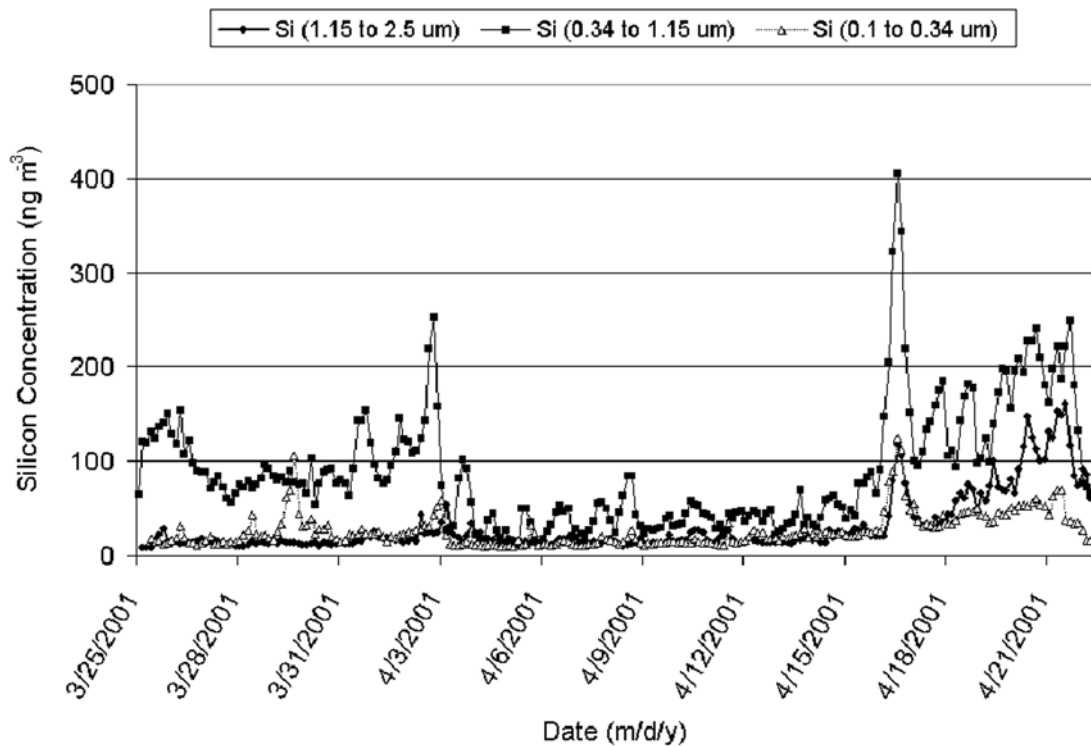


Figure 14. Fine-, medium-, and large-size fraction silicon at Poker Flat from 25 March to 22 April 2001. Other crustal elements sampled show similar size fractionation time series.

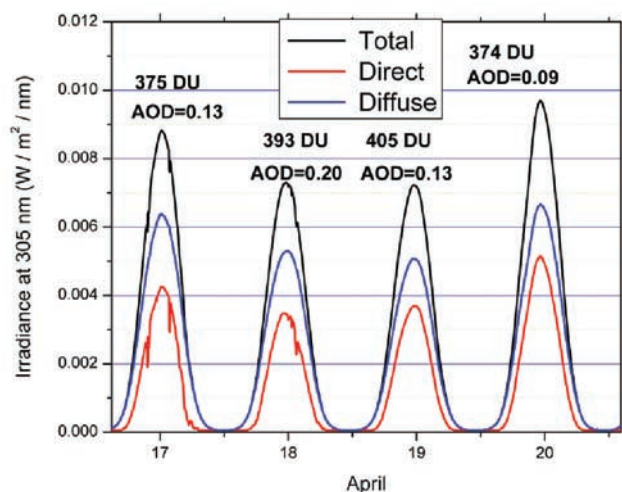


Figure 15. Spectral irradiances measured at Poker Flat, Alaska, during mid April 2001, with midday values of ozone column amount (DU) and aerosol optical depth (AOD_{368}) obtained from the UV MFRSR instrument.

what greater UV absorption for the larger particles than in the small-size range.

[31] The AOD_{368} during the period of the Asian air mass influence varied in the range 0.12–0.21. The overall UV impact of aerosol fluctuations can be evaluated in terms of other factors that can influence scattering and absorption, such as ozone variations which strongly impact transmittance at the shorter UV wavelengths. A decrease in aerosol

extinction can mask the effect of an ozone increase. Spectral irradiances measured at 305 nm during 4 consecutive days in this period are shown in Figure 15, with annotation to indicate the ozone column amount and aerosol optical depth values determined at midday from the UV-MFRSR measurements. The increase in ozone amount from 18 April (393 DU) to 19 April (405 DU) during a period of peak aerosol concentration is not accompanied by a notable decrease in UV irradiance, evidently because of the compensating effect from decreased AOD. Model sensitivity studies using measurements are valuable in assessing the relative magnitudes of competing parameters. For example, although there were nearly identical column ozone amounts on 17 April (375 DU) and 20 April (374 DU), the total irradiance on 20 April was $\sim 10\%$ higher than that of 17 April. Both the AOD and changing solar zenith angle between the two dates contribute to this increase, but AOD produces the majority of the effect.

3.3.4. Marine Air Mass

[32] The period 3–15 April 2001 was cloudy in central and southern Alaska. Incoming air was transported northward from the Gulf of Alaska and passed through deep convective cloud systems. The air mass in the Gulf of Alaska had likely entrained some of the Asian dust that was transported into the Gulf following the high wind event of 6–7 April over Mongolia. Aerosol concentrations were variable and were at times low (Figure 3) because of precipitation scavenging along the transport pathway. The SMPS size distribution is bimodal as shown in Figure 16. The larger of the two modes detected by the SMPS is likely to be residue from the evaporation of cloud droplets and precipitation. The gap between the modes corresponds to

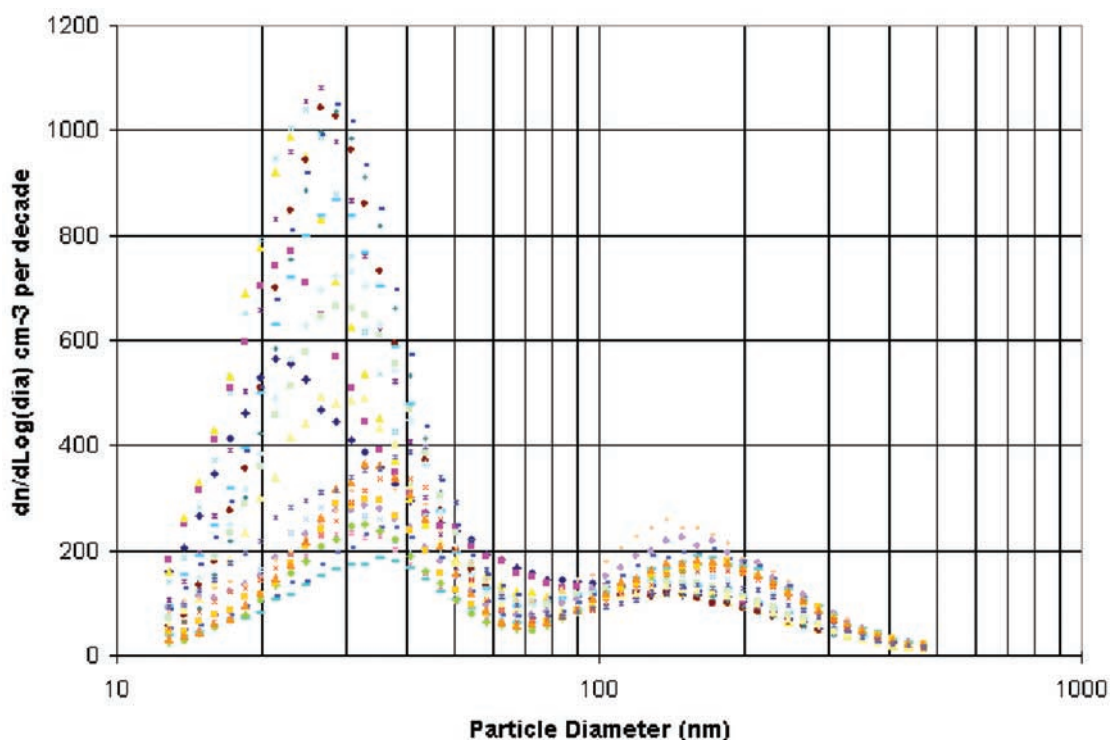


Figure 16. A series of aerosol size distributions on 12 April 2001 representing a cloud-processed marine air mass sampled at Poker Flat, Alaska, indicating a bimodal distribution with large concentrations in the nucleation size range.

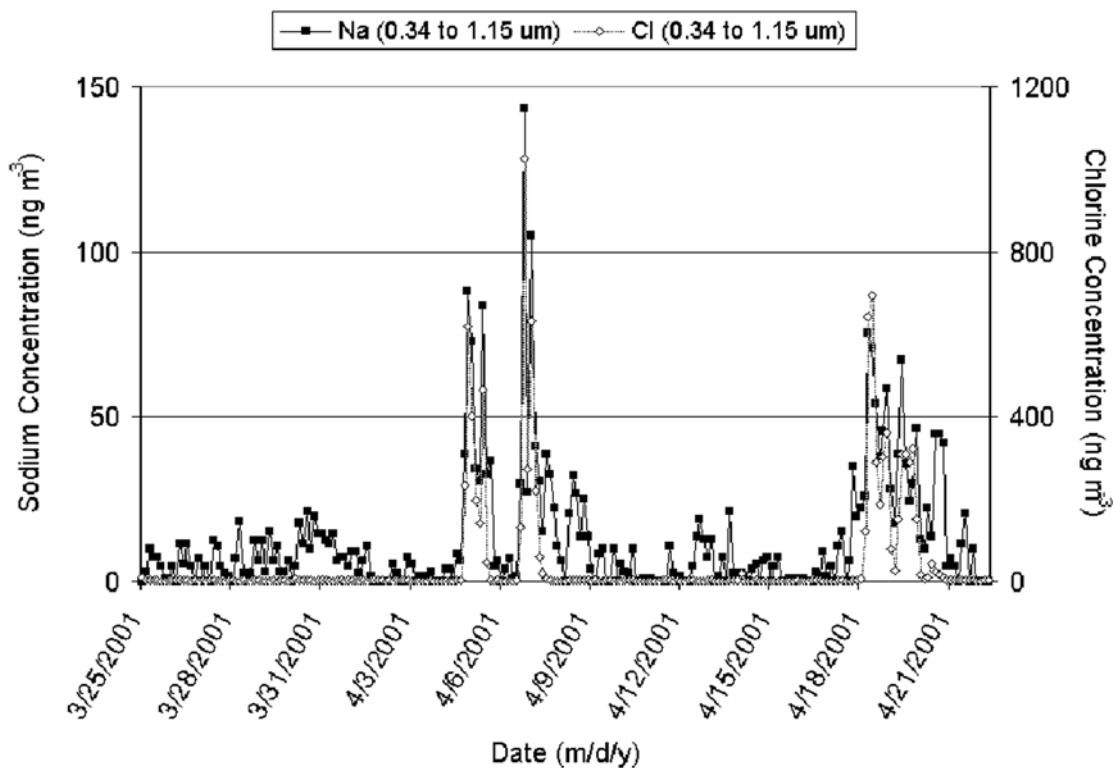


Figure 17. Medium-size fraction sodium and chlorine at Poker Flat from 25 March to 22 April 2001.

minimum size of aerosols activated during cloud formation. This gap is typically located near 50 nm diameter, which corresponds to aerosol activation at a maximum supersaturation of a few tenths of one percent [Pruppacher and Klett, 1978]. The smaller mode of particles is in the size range for gas-to-particle production that typically occurs in “bursts” within a humid, sunlit environment, attributed in this case to sulfur precursor gases from biogenic sources known to be significant in the Gulf of Alaska region.

[33] During breaks in cloud cover the optical depths could be derived and were estimated in the range 0.05–0.25 at 368 nm, indicating a wide range of aerosol conditions. The larger values occurred during periods of high relative humidity. The time series of aerosol concentrations indicates large variability in the 0.3–0.5 μm diameter range and pulses of large aerosol (diameter $>1 \mu\text{m}$) at magnitudes similar to those of the Asian dust episode in mid April. Modeled UV transmittance for 9 April during a period of elevated AOD was 89–90% of the UV calculated for nonaerosol conditions (Table 1). The estimated aerosol SSA this day was 0.95 (Table 3), consistent with a predominantly sulfate aerosol composition.

[34] Chemical analysis detected both Na and Cl at elevated levels in the medium and large-size fractions (Figure 17) suggest a marine source of aerosol, corresponding to an air parcel trajectory primarily over open ocean. However, the trajectory also passed for approximately 300 km over land and the aerosol composition includes some soil elements (Figure 5). During this period, the total relative aerosol absorption was low except for a period of elevated absorption that occurred 8–9 April (Figure 13). The spectral absorption measurements indicate slightly greater relative

absorption in the UV (350 nm) than the visible or near-infrared wavelengths for the large particles but smaller UV effects for small aerosol.

4. Summary and Discussion

[35] Four aerosol source types were selected to characterize their physical, optical and chemical properties for use in analysis of data from a UV monitoring site for central Alaska. During a period when aerosol chemistry and air parcel trajectory information suggested Arctic haze composition, AOD_{368} values remained <0.1 as in a comparative period in September. This was attributed to small mass loading in the air parcel by the time it crossed the northern mountain ranges and reached central Alaska. The aerosol in these conditions has little interaction with the UV radiation field, decreasing the UV spectral transmittance by only 0.03 compared with no-aerosol model calculations. Analysis was also conducted for aerosol loading with dust and industrial particulates originating in Asia and crossing the northern Pacific. These aerosols were primarily sulfur and crustal compounds, with trace quantities of heavy metals. The total UV transmittance for the Asian dust event was reduced by 0.05 compared to no-aerosol simulations and the AOD_{368} was moderate (0.13), but total aerosol absorption was significantly larger than for the Arctic or marine air mass periods. Aerosol in a marine air mass was associated with large AOD (up to 0.25) at UV wavelengths and a 0.10 decrease in UV spectral transmittance, but these effects can be attributed to growth of the aerosol in a humid environment, and the impactor samples of this aerosol had low absorption compared to the Asian dust period. UV absorp-

tion was measured in three size ranges for the aerosol impactor samples, and appears to be relatively more effective for the populations of larger particles.

[36] The presence of aerosol in the long slant pathway of the direct solar beam allows enhanced extinction through both scattering and absorption. Although the mass loading of aerosol is often small in this geographic region, the aerosol types are effective at interacting with near-UV light [Shaw, 1987]. Relatively small concentrations of aerosol can have an impact on the UV radiation field that is comparable to ozone fluctuations. Both the repartitioning of UV radiation between the direct beam and diffuse components, and size- or chemistry-dependent UV absorption properties, have ramifications for ozone trend monitoring, photochemical process modeling, sensitivity to surface albedo and multiple scattering between clouds and the surface, and use of spectral measurements and models to calculate UV biological response functions for humans or other organisms. The radiative, aerosol, and meteorological measurements at Poker Flat are ongoing and will continue to provide data for assessment of links between atmospheric conditions and UV exposure trends in this high-latitude region.

[37] **Acknowledgments.** This research was funded by grants from NOAA (NA67RJ0146; NA67RJ0147), NSF (OPP-0002239) and the University of Alaska (UAF) International Arctic Research Center program on Global Change in the Arctic (grants 02-0012 and FP100947). Additional support was provided by the U.S. Department of Agriculture (USDA). The authors wish to thank the staff of the UAF Poker Flat Research Range for their support during the field program, the University of California, Davis, DELTA Group, and George Janson, Bill Durham, and Gwen Scott of the USDA UV-B Program Office at Colorado State University Natural Resources Ecology Laboratory. The HYSPLIT4 (Hybrid Single-Particle Lagrangian Integrated Trajectory) Model was utilized for air parcel trajectory information (web address: <http://www.arl.noaa.gov/ready/dispersion.html>, NOAA Air Resources Laboratory, Silver Spring, MD, USA). Any opinions, findings, and conclusions or recommendations expressed in this material are those of the authors and do not necessarily reflect the views of the sponsors.

References

- Bigelow, D. S., J. R. Slusser, A. F. Beaubien, and J. H. Gibson, The USDA Ultraviolet Radiation Monitoring Program, *Bull. Am. Meteorol. Soc.*, **79**, 601–615, 1998.
- Bjorn, L. O., Effects of ozone depletion and increased UV-B on terrestrial systems, *Int. J. Environ. Stud.*, **51**, 217–243, 1996.
- Bojkov, R. D., D. S. Balis, and C. S. Zerefos, Characteristics of the ozone decline in the northern polar and middle latitudes during the winter-spring, *Meteorol. Atmos. Phys.*, **69**, 119–135, 1998.
- Booth, C. R., T. B. Lucas, and J. H. Morrow, High-resolution ultraviolet spectral irradiance monitoring program in polar regions: Six years (and growing) of data available to polar researchers in ozone- and ultraviolet-related studies, *Antarct. J. U. S. Rev.*, **1993**, 338–341, 1994.
- Cahill, T. A., S. S. Cliff, K. D. Perry, M. P. Jimenez-Cruz, and S. A. McHugo, Size and time resolved anthropogenic components of aerosols via synchrotron x-ray fluorescence: Application to Asian aerosol transport, *Eos Trans. AGU*, **80**(46), Fall Meet. Suppl., F148, 1999.
- Campbell, D., S. Copeland, and T. Cahill, Measurement of aerosol absorption coefficient from Teflon filters using integrating plate and integrating sphere techniques, *Aerosol Sci. Technol.*, **22**, 287, 1995.
- Climate Monitoring and Diagnostics Laboratory, Summary report no. 26, Boulder, Colo., 2002.
- Estupinan, J. G., S. Raman, G. H. Crescenti, J. J. Streicher, and W. F. Barnard, Effects of cloud and haze on UV-B radiation, *J. Geophys. Res.*, **101**(D11), 16,807–16,816, 1996.
- Frederick, J. E., and H. D. Steele, The transmission of sunlight through cloudy skies: An analysis based on standard meteorological information, *J. Appl. Meteorol.*, **34**, 2755–2761, 1995.
- Gao, W., J. R. Slusser, J. Gibson, G. Scott, D. S. Bigelow, J. Kerr, and B. McArthur, Direct-Sun column ozone retrieval by the UV multi-filter rotating shadow-band radiometer and comparison with those from Brewer and Dobson spectrophotometers, *Appl. Opt.*, **40**(19), 3149–3155, 2001.
- Gurney, K. R., Evidence for increasing ultraviolet irradiance at Point Barrow, Alaska, *Geophys. Res. Lett.*, **25**(6), 903–906, 1998.
- Hansen, G., and M. P. Chipperfield, Ozone depletion at the edge of the Arctic polar vortex: 1996/1997, *J. Geophys. Res.*, **104**(D1), 1837–1845, 1999.
- Harrison, L., and J. Michalsky, Objective algorithms for the retrieval of optical depths from ground-based measurements, *Appl. Opt.*, **33**, 5126–5132, 1994.
- Harrison, L., J. Michalsky, and J. Berndt, Automated multi-filter rotating shadowband radiometer—An instrument for optical depth and radiation measurements, *Appl. Opt.*, **33**, 5118–5125, 1994.
- Helbling, E. W., and V. E. Villafane, UV radiation effects on phytoplankton primary production: A comparison between Arctic and Antarctic marine ecosystems, in *UV Radiation in Arctic Ecosystems*, edited by D. O. Hessen, Springer-Verlag, New York, 2002.
- Herman, J. R., P. K. Bhartia, J. Ziemeke, Z. Ahmad, and D. Larko, UV-B increases (1979–1992) from decreases in total ozone, *Geophys. Res. Lett.*, **23**(16), 2117–2120, 1996.
- Herman, J. R., N. Krotkov, E. Celarier, D. Larko, and G. Labow, Distribution of UV radiation at the Earth's surface from TOMS-measured UV-backscattered radiances, *J. Geophys. Res.*, **104**(D10), 12,059–12,076, 1999.
- Hofzumahaus, A., A. Kraus, A. Kylling, and C. S. Zerefos, Solar actinic radiation (280–420 nm) in the cloud-free troposphere between ground and 12 km altitude: Measurements and model results, *J. Geophys. Res.*, **107**(D18), 8139, doi:10.1029/2001JD900142, 2002.
- Kylling, A., T. Persen, B. Mayer, and T. Svenoe, Determination of an effective spectral surface albedo from ground-based global and direct UV irradiance measurements, *J. Geophys. Res.*, **105**(D4), 4949–4959, 2000.
- Li, J., J. G. D. Wong, J. S. Dobbie, and P. Chylek, Parameterization of the optical properties of sulfate aerosols, *J. Atmos. Sci.*, **58**, 193–209, 2001.
- Madronich, S., and F. R. de Grujil, Skin cancer and UV radiation, *Nature*, **366**, 23, 1993.
- Minschwaner, K., New observations of ultraviolet radiation and column ozone from Socorro, New Mexico, *Geophys. Res. Lett.*, **26**(8), 1173–1176, 1999.
- Perry, K. D., T. A. Cahill, R. C. Schnell, and J. M. Harris, Long-range transport of anthropogenic aerosols to the NOAA Baseline Station at Mauna Loa Observatory, Hawaii, *J. Geophys. Res.*, **104**(D15), 18,521–18,533, 1999.
- Petters, J. L., V. K. Saxena, J. R. Slusser, B. N. Wenny, and S. Madronich, Aerosol single scattering albedo retrieved from measurements of surface UV irradiance and a radiative transfer model, *J. Geophys. Res.*, **108**(D9), 4288, doi:10.1029/2002JD002360, 2003.
- Pruppacher, H. R., and J. D. Klett, *Microphysics of Clouds and Precipitation*, D. Reidel, Norwell, Mass., 1978.
- Quinn, P. K., T. L. Miller, T. S. Bates, J. A. Ogren, E. Andrews, and G. E. Shaw, A 3-year record of simultaneously measured aerosol chemical and optical properties at Barrow, Alaska, *J. Geophys. Res.*, **107**(D11), 4130, 10.1029/2001JD001248, 2002.
- Rahn, K. A., R. D. Borys, and G. E. Shaw, Asian source of Arctic haze bands, *Nature*, **268**, 713–715, 1977.
- Reuder, J., and H. Schwander, Aerosol effects on UV radiation in nonurban regions, *J. Geophys. Res.*, **104**(D4), 4065–4077, 1999.
- Shaw, G. E., On the climatic relevancy of Arctic haze: Static energy balance considerations, *Tellus, Ser. B*, **37**(1), 50–52, 1985.
- Shaw, G. E., Aerosols as climate regulators: A climate-biosphere linkage?, *Atmos. Environ.*, **21**, 985–986, 1987.
- Shaw, G. E., Chemical air mass systems in Alaska, *Atmos. Environ.*, **22**, 2239–2248, 1988.
- Shaw, G. E., The Arctic haze phenomenon, *Bull. Am. Meteorol. Soc.*, **76**, 2403–2413, 1995.
- Shaw, G. E., K. Stamnes, and Y. X. Hu, Arctic haze: Perturbation to the radiation field, *Meteorol. Atmos. Phys.*, **51**, 227–235, 1993.
- Shindell, D. T., D. Rind, and P. Lonergan, Increased polar stratospheric ozone losses and delayed eventual recovery owing to increasing greenhouse-gas concentrations, *Nature*, **392**, 589–592, 1998a.
- Shindell, D. T., D. Rind, and P. Lonergan, Climate change and the middle atmosphere. part IV: Ozone response to doubled CO₂, *J. Clim.*, **11**(5), 895–918, 1998b.
- Slusser, J. R., J. H. Gibson, D. Kolinski, P. Disterhoff, K. Lantz, and A. F. Beaubien, Langley method of calibrating UV filter radiometers, *J. Geophys. Res.*, **105**, 4841–4849, 2000.
- Slusser, J. R., N. Krotkov, W. Gao, J. R. Herman, G. Labow, and G. Scott, Comparisons of USDA UV shadow-band irradiance measurements with

- TOMS satellite and DISORT model retrievals under all sky conditions, *Proc. SPIE Int. Soc. Opt. Eng.*, 4482, 56–63, 2002.
- Sokolik, I. N., and O. B. Toon, Incorporation of mineralogical composition into models of the radiative properties of mineral aerosol from UV to IR wavelengths, *J. Geophys. Res.*, 104(D8), 9423–9444, 1999.
- Solomon, S., Stratospheric ozone depletion: Review of concepts and history, *Rev. Geophys.*, 37(3), 275–316, 1999.
- Stamnes, K., S.-C. Tsay, W. Wiscombe, and K. Jayaweera, Numerically stable algorithm for discrete ordinate method radiative transfer in multiple scattering and emitting layered media, *Appl. Opt.*, 27, 2502–2509, 1988.
- Taalas, P., J. Damski, E. Kyro, G. Esko, and M. Ginzburg, Effect of stratospheric ozone variations on UV radiation and on tropospheric ozone at high latitudes, *J. Geophys. Res.*, 102(D1), 1533–1539, 1997.
- Torres, O., P. K. Bhartia, J. R. Herman, Z. Ahmad, and J. Gleason, Derivation of aerosol properties from satellite measurements of backscattered ultraviolet radiation: Theoretical basis, *J. Geophys. Res.*, 103(D14), 17,099–17,110, 1998.
- United Nations Environment Programme (UNEP), *Environmental Effects of Ozone Depletion: 1998 Assessment*, Elsevier Sci., New York, 1998.
- Weihs, P., et al., Modeling the effect of an inhomogeneous surface albedo on incident UV radiation in mountainous terrain: Determination of an effective surface albedo, *Geophys. Res. Lett.*, 28(16), 3111–3114, 2001.
- Wenny, B. N., J. S. Schafer, J. J. DeLuisi, V. K. Saxena, W. F. Barnard, I. V. Petropavlovskikh, and A. J. Vergamini, A study of regional aerosol radiative properties and effects on ultraviolet-B radiation, *J. Geophys. Res.*, 103(D14), 17,083–17,097, 1998.
- World Meteorological Organization, *Scientific Assessment of Ozone Depletion*, Rep. Global Ozone Res. and Monit. Proj., no. 44, Geneva, Switzerland, 1999.
-
- R. D. Borys and M. A. Wetzel, Division of Atmospheric Sciences, Desert Research Institute, Reno, NV 89512, USA. (wetzel@dri.edu)
- C. F. Cahill and G. E. Shaw, Geophysical Institute, University of Alaska, Fairbanks, AK 99775, USA.
- J. R. Slusser, Natural Resources Ecology Laboratory, Colorado State University, Fort Collins, CO 80523, USA.